The Cryosphere Discuss., 8, 3237–3261, 2014
www.the-cryosphere-discuss.net/8/3237/2014/
doi:10.5194/tcd-8-3237-2014

The Cryosphere Discussions
Open Access

Detailed ice loss pattern in the northern Antarctic Peninsula: widespread decline driven by ice front retreats

T. A. Scambos[1], E. Berthier[2], T. Haran[1], C. A. Shuman[3], A. J. Cook[4], S. R. M. Ligtenberg[5], and J. Bohlander[1]

[1]National Snow and Ice Data Center (NSIDC), University of Colorado at Boulder, Boulder CO 80303, USA
[2]Laboratoire d'Etudes en Géophysique et Océanographie Spatiales, Centre National de la Recherche Scientifique (LEGOS CNRS), Université de Toulouse, Toulouse 31400, France
[3]University of Maryland, Baltimore County, Joint Center for Earth Technology (UMBC JCET) at NASA Goddard Space Flight Center, Greenbelt, MD 20771, USA
[4]Department of Geography, Swansea University, Swansea SA2 8PP, UK
[5]Institute for Marine and Atmospheric Research Utrecht (IMAU), Utrecht 3508 TA, the Netherlands

Received: 3 June 2014 – Accepted: 4 June 2014 – Published: 18 June 2014

Correspondence to: T. A. Scambos (teds@nsidc.edu)

Published by Copernicus Publications on behalf of the European Geosciences Union.

Abstract

The northern Antarctic Peninsula (nAP, $< 66^{\circ}$ S) is one of the most rapidly changing glaciated regions on Earth, yet the spatial patterns of its ice mass loss at the glacier basin scale has to date been poorly documented. We use satellite laser altimetry and satellite stereo-image topography spanning 2001–2010 to map ice elevation change and infer mass changes for 33 glacier basins. Rates of ice volume and ice mass change are $27.7 \pm 8.6\,\mathrm{km}^3\,\mathrm{a}^{-1}$ and $24.9 \pm 7.8\,\mathrm{Gt\,a}^{-1}$. This mass loss is compatible with recent gravimetric assessments, but it implies that almost all the gravimetry-inferred loss lies in the nAP sector. Mass loss is highest for eastern glaciers affected by major ice shelf collapses in 1995 and 2002, where twelve glaciers account for 60 % of the total imbalance. However, losses at smaller rates occur throughout the nAP, and at high and low elevation, despite increased snow accumulation along the western coast and at high elevations. We interpret the widespread mass loss to be driven by decades of ice front retreats on both sides of the nAP, and by the propagation of kinematic waves triggered at the fronts into the interior.

1 Introduction

The nAP is one of two key areas of the Antarctic Ice Sheet showing major mass loss, the other being the Amundsen Sea region. Previous studies have shown large negative mass imbalances and significant elevation losses for the nAP (Ivins et al., 2011; Shepherd et al., 2012; Luthcke et al., 2013; Sasgen et al., 2013; McMillan et al., 2014), but in general these have not resolved the spatial distribution of the mass balance change in detail. Studies based on gravitational change detection using the Gravity Recovery and Climate Experiment satellite system (GRACE) have an inherent spatial resolution of roughly 250 km scale (Ivins et al., 2011; Luthcke et al., 2013; Sasgen et al., 2013), far larger than the scale of the nAP individual glacier basins and islands. Past altimetry-based studies (Pritchard et al., 2009; Flament and Rémy, 2012; Shepherd et al., 2012)

TCD
8, 3237–3261, 2014

suffer from either sparse coverage or slope correction issues, or both, due to the steep terrain in the nAP. In the published assessments based on laser altimetry (Shepherd et al., 2012), severe assumptions and large extrapolations are required to interpolate the data across the entire region. Mass budget methods (Rignot et al., 2004, 2008; Rott et al., 2011; Shepherd et al., 2012), which aim to difference outflowing ice flux and surface mass balance (SMB) for each glacier basin have to date shown results that are difficult to reconcile with other studies of the same glaciers (Shuman et al., 2011; Berthier et al., 2012). This is primarily due to spatially coarse SMB estimates from models or field measurements, difficulties in estimating the cross-sectional area of the glaciers, and differences in the span of time used to estimate ice flux changes (Berthier et al., 2012).

The goal of this study is to determine the spatial pattern of ice elevation changes in the nAP, improve estimates of mass balance for the region, and study the relationship of mass balance with ice shelf collapse and ice front retreats in the area. In light of known climate changes in the region, such as air warming, regional sea ice decline, and increasing accumulation (e.g., Mulvaney et al., 2012; Zagorodnov et al., 2012; Stammerjohn et al., 2008; Lenaerts et al., 2012), our study reveals a pattern of ice mass loss in space and (we infer) time that may represent the characteristics of mass loss in other areas of Antarctica in the coming century.

2 Methods

Our study combines satellite stereo-image digital elevation model differencing (dDEM) with repeat-track laser altimetry from the Ice, Cloud and land Elevation Satellite (ICESat; Shutz et al., 2005), with the objective of providing an assessment of vertical movement resolved at the scale of the major glacier catchments. We use stereo-image data from Advanced Spaceborne Thermal Emission and Reflection Radiometer (ASTER; Fujisada et al., 2005) and Satellite Pour l'Observation de la Terre 5 (SPOT5; Korona et al., 2009). Eight satellite stereo-image data sets from the ASTER sensor, and six

TCD
8, 3237–3261, 2014

from the SPOT-5 Haute Résolution Stéréoscopique (HRS) sensor (Supplement Table S1 and Fig. S1) were processed using previously published methods (Shuman et al., 2011; Berthier et al., 2012; Gardelle et al., 2013).

For the ICESat repeat-track data (Release 633), we used 26 ground tracks from the 91-day-repeat orbit crossing the nAP and major ice-covered islands for the high-energy laser campaigns (ICESat Laser 2A through Laser 3J, September 2003–March 2008; Shuman et al., 2006). Cross-track elevation adjustment and along-track filtering are used to improve measurement quality, based on surface slopes (not elevations) derived from a recent Antarctic Peninsula DEM (Cook et al., 2012). We first eliminated ICESat profile tracks more than 300 m from the reference track position, and sections where the absolute slope from the gridded DEM was $> \pm 10$ % slope, or $\pm 5.7^{\circ}$ for the reference track or measurement track location, or areas where the absolute difference between along-track slopes of the measurement track and reference track exceeded 5 % (or $\pm 2.86^{\circ}$). We further required the ICESat elevation data to be within 50 m (vertically) of the corresponding interpolated DEM elevation. All elevations are referenced to the EGM96 geoid datum. To migrate the track data to the reference track and compare elevations, we identified reference track "stations" every 43.75 m along the reference track (one-fourth the distance between ICESat altimetry shot locations along track). We then applied an elevation correction based on the difference between the interpolated gridded DEM elevation at the nearest reference track station and the ICESat track data point. ICESat campaign data were compared by differencing their migrated elevations, divided by the time in years between dates of track acquisition. To reduce effects of possible seasonal variations in elevation, we compared only near-integer-year separated repeat profiles, e.g., data from campaigns 2A to 3A ($\sim$ October, $\sim$ 1 year apart) or 3B to 3H ($\sim$ March, $\sim$ 2 years apart).

To evaluate different processes in elevation and ice mass change, we treat regions above and below 1000 m a.s.l. separately for each of 33 drainage basins. This is the approximate elevation of an extensive escarpment in the nAP separating a plateau area from individual glacier cirques. Above 1000 m a.s.l., and for islands without sufficient

TCD
8, 3237–3261, 2014

dDEM coverage (Robertson Is., Snow Hill Is., and Joinville, Dundee, and D'Urville Is.; Fig. 1), the rate of elevation change (dH/dt) is determined from satellite laser altimetry alone. In smooth high elevation areas, correlation of satellite stereo-images often fails due to a lack of high-contrast surface features of sufficient horizontal scale (tens of meters). Below 1000 m a.s.l., a hypsometric interpolation method was applied to individual glaciated basins to extend differencing of satellite stereo-image DEMs (dDEM) and ICESat dH/dt measurements to areas not directly measured. ICESat dH/dt was weighted 10-fold relative to dDEM dH/dt to prevent small image areas from dominating the dH/dt mapping and to reflect the higher accuracy of individual ICESat-based measurements, using

$$(\mathrm{d}H/\mathrm{d}t_{\mathrm{DEM}} \cdot (N_{\mathrm{DEM}}/e_{\mathrm{DEM}}) + \mathrm{d}H/\mathrm{d}t_{\mathrm{ICESat}} \cdot (N_{\mathrm{ICESat}}/e_{\mathrm{ICESat}}))/ ((N_{\mathrm{DEM}}/e_{\mathrm{DEM}}) + (N_{\mathrm{ICESat}}/e_{\mathrm{ICESat}})) \quad (1)$$

where N is the number of measurements (50 m grid cells for the dDEMs; shot point locations at the 43.75 m spacing for ICESat) and e is an inverse weighting of the measurement methods. For dDEMs we used a weight of 1, and for ICESat, we used 0.1. This allowed the fewer but more accurate ICESat-based measurements to contribute to the final result in basins with extensive dDEM coverage. ICESat data were often in regions not well covered by dDEM results.

We also estimate the above-flotation mass loss of grounded-ice areas that retreated at least 2 km^2 during the study interval (2001–2010), as identified by image mapping (Cook et al., 2005; Cook and Vaughan, 2010). To estimate the volume and mass loss represented by these areas we mapped the area of retreat during our study period (2002–2010) and half the mean elevation loss rate observed just above the area of grounded ice retreat. This represents an assumption that the vertical elevation change rate of the retreated ice was identical to the region just upstream of the loss area, and that the time of ice front retreat (e.g., when the ice calved and drifted away) was midway through the study period.

TCD
8, 3237–3261, 2014

Errors for our assessment of dH/dt (Tables 1 and Supplement Table S2), are based on past analysis of the dDEM method (Shuman et al., 2011; Berthier et al., 2012), on inter-comparisons of the two methods at sites having both dDEM and ICESat measurements, and on crossover analysis of ICESat cross-track-corrected data (Supplement Table S4). Past analysis for this region suggests that dDEM methods using mixed ASTER and SPOT5 imagery can have a ±5 m uncertainty for individual glacier basin, i.e. $\sim 1\,\mathrm{m\,a^{-1}}$ given a 5 yr time separation between DEMs. However, examining our ICESat and dDEM dH/dt at sites with both measurements (6158 sites) shows that the methods differ by just $\sim 0.3\,\mathrm{m\,a^{-1}}$ overall, and range between 0.07 to $0.75\,\mathrm{m\,a^{-1}}$ over various sub-sets of our measurements (Supplement Table S4). This is in agreement with our previous study that showed reduced errors when dDEM results are averaged over basin-scale areas (Berthier et al., 2012). Seven crossover sites with slope-corrected ICESat dH/dt measurements show good agreement with the dDEM measurements at the same locations (mean offset of $+0.05\,\mathrm{m\,a^{-1}}$).

Errors in the ICESat cross-track correction for dH/dt are more dependent on slope errors in the gridded Cook et al. (2012) DEM and not its absolute elevation accuracy. Assuming our selection criteria eliminated regions of significant error in the gridded DEM, we estimate that across-track or along-track slopes in the Cook et al. (2012) DEM are accurate to within ±0.5° over a length scale of 300 m, or $\pm 8.7\,\mathrm{m\,km^{-1}}$. A test of this was conducted by comparing the Cook et al. (2012) DEM slopes with a DEM acquired in 2009 by the NASA Land, Vegetation, and Ice Sensor (LVIS) airborne laser altimeter, covering about 20 % of the study region. This showed that the mean difference in along-track slope in the overlap region was 0.06 ± 1.2° when our criteria are applied to both data sets. For laser altimetry measurements alone, our inferred mean slope error of ±0.5° implies a mean laser measurement pair cross-track correction error of ±1.31 m (assuming a mean cross-track distance of 150 m). We assume this error is randomly distributed when averaging a glacier basin. Thus for the average of 20 measurement sites, the mean error is < 25 cm. Since laser measurement pairs may have 1 to 4 years separation in time, our overall mean error in elevation change rate is significantly less

TCD
8, 3237–3261, 2014

than this. Additionally, the majority of the basins we consider have many more than 20 measurement sites.

Considering all sources of error, and variations in the time-span of measurements for dDEM and ICESat measurements, data density variations for the basins, and the strong agreement between these independent altimetric methods, we adopt a mean error of $\pm 0.15\,\mathrm{m\,a^{-1}}$ for regions of laser altimetry measurement alone (above 1000 m a.s.l.), and $\pm 0.3\,\mathrm{m\,a^{-1}}$ for our dDEM plus altimetry measurements (below 1000 m a.s.l.) and the glacier basins, islands, and sub-basins without laser altimetry. Errors for volume and mass change determinations thus scale with area.

3 Results

An overview of our results is shown in Fig. 2 and Table 1, and detailed basin-by-basin values and patterns are provided in Supplement Table S2. The results show that basins impacted by recent ice shelf loss and ice front retreat have very high rates of change, but also indicate that few areas – high or low, east or west – have positive $\mathrm{d}H/\mathrm{d}t$. Ice-shelf loss (ISL) basins, all on the eastern side of the nAP, and four smaller areas of grounded ice front loss (IFL) on the western and northeastern side of the nAP, show a characteristic pattern of very high elevation loss rates just upstream of the ice front but far lower elevation losses at high elevation. Mean elevation change for areas below 1000 m a.s.l. at 12 eastern-side ISL glacier basins (or sub-basins) is $-2.6\,\mathrm{m\,a^{-1}}$ (range, +0.4 to $-5.8\,\mathrm{m\,a^{-1}}$) and $-2.2\,\mathrm{m\,a^{-1}}$ (-2.0 to $-2.7\,\mathrm{m\,a^{-1}}$) for the four western-side and northeastern IFL sub-basins experiencing recent ice front retreat ($>2\,\mathrm{km^2}$ since 2000). At elevations >1000 m, elevation loss in all the eastern ISL basins is small (mean, $-0.10\,\mathrm{m\,a^{-1}}$; range +0.35 to $-0.54\,\mathrm{m\,a^{-1}}$). Glacier systems on the western nAP coast and the western islands below 1000 m a.s.l., excluding the recent IFL regions, are changing at variable rates (typically $\sim -0.15\,\mathrm{m\,a^{-1}}$, range +0.7 to $-1.6\,\mathrm{m\,a^{-1}}$). However, these western-side basins are losing elevation at significant rates above 1000 m a.s.l. (mean of $-0.59\,\mathrm{m\,a^{-1}}$; range -0.25 to $-1.30\mathrm{m\,a^{-1}}$).

TCD
8, 3237–3261, 2014

We examine the rates of surface elevation change and cumulative ice volume change as they vary with altitude for three sub-regions of the study area in Fig. 3. The patterns of elevation change with altitude illustrate the differences between the western-side glacier and island regions and the eastern-side ISL areas, and also highlight the bi-modal hypsometry pattern characteristic of the nAP. Eastern-side ISL areas show dramatically decreasing elevation with time, and large volume changes at low elevations, and little or no significant change in the upper-most catchment areas (Fig. 3c and d). Western-side glaciers show mildly negative rates of elevation change at all elevations, and a steady cumulative volume decrease rate with altitude. The major glaciers of Scar Inlet Ice Shelf, the lone remaining large ($> 50\,km^2$) ice shelf in the study area with significant tributary glaciers, show a unique pattern of ice losses at low elevation and some areas of thickening at altitude. We believe this is likely the pattern of elevation change present for the eastern nAP ISL glacier systems in the years prior to shelf disintegration.

4 Discussion

The widespread elevation losses suggested here for both sides of the nAP at high elevations, and especially for the western side of the divide, have significant implications for its recent mass change history. Previous observational studies have shown that the elevation decline pattern for ISL or IFL glaciers migrates upstream and diffuses on a scale of years to decades (Howat et al., 2007; Joughin et al., 2008; Shuman et al., 2011; Berthier et al., 2012), consistent with kinematic wave models of glacier response to ice front stress changes for tidewater glaciers (Pfeffer, 2007; Nick et al., 2009; Favier et al., 2014). In past work (Shuman et al., 2011; Berthier et al., 2012) and in these results we observe that eastern ISL glaciers are currently propagating kinematic waves upstream from their lower trunk areas, but this process has not yet had a significant impact on higher elevations. Western-coast nAP glacier front retreats, elevation losses, and accelerations have been documented (Cook and Vaughan, 2005;

TCD
8, 3237–3261, 2014

Pritchard and Vaughan, 2007; Kunz et al., 2012), with a major pulse of retreat beginning in the 1970s. Moreover, our work here shows that on-going ice front losses within the study period behave much like smaller versions of the eastern-side glaciers impacted by ice shelf and glacier front retreat (Table 1). The earlier losses inferred for the western side fjord glaciers (e.g., Crist et al., 2014) appear to have now propagated throughout the entirety of the western basins, leading to significant and widespread surface lowering in the western upper catchment areas (> 1000 m a.s.l.) at greater rates than for the eastern side on average (Table 1 and Supplement Table S2).

However, any measurement of elevation or mass losses along the western coast and in the upper elevation areas must be reconciled with a large recent positive accumulation anomaly. Ice cores at two sites on the nAP ridge crest (Detroit Plateau, 64.08° S, 59.65° W, 1937 m a.s.l., and Site Beta of the Larsen Ice Shelf System, Antarctica, 66.03° S, 64.04° W, 1980 m a.s.l.; Fig. 1) show significant increases in accumulation in the late 20th century: 2052 to 2776 kg m^2 a^{-1} from 1981–1987 to 2001–2007, and 1750 to 2710 kg m^2 a^{-1} from 1960–1969 to 2000–2008, respectively (Potocki et al., 2011; Goodwin, 2013). Models of precipitation input for the region (Saha et al., 2010; Dee et al., 2011; Lenaerts et al., 2012) also show a strong overall increase for the most recent decades, but some indicate a slight decline in the last decade, covering our dH/dt measurement period (Saha et al., 2010; Lenaerts et al., 2012; Shepherd et al., 2012). The large increase and later reduction in accumulation are associated with multi-decadal warming (Barrand et al., 2013) and associated reductions in sea ice extent northwest of the nAP (Stammerjohn et al., 2012) recently moderated by a slight cooling trend (Blunden and Arndt, 2012; Zagorodnov et al., 2012).

Multi-decadal accumulation, temperature and snowmelt trends cause changes in the compaction rate of snow and firn, and can potentially impact measurements of surface elevation change (Ligtenberg et al., 2011). Using a model climate time series (based on reanalysis of weather data) spanning the period of our measurements (RACMO-2.1/ANT; Lenaerts et al., 2012), a dH/dt for the firn column at 27 km spatial scale is obtained similar to that used in previous related analyses (Pritchard et al., 2012;

TCD
8, 3237–3261, 2014

Gardner et al., 2013). The modelled inter-annual variability in accumulation, temperature and snowmelt, and their effect on firn compaction result in dH/dt corrections between −0.19 to +0.12 m a^{-1} on the grounded ice of the nAP, with generally positive (thickening) corrections on the western side and negative to the east. The small effect on the firn layer, and the high variability of accumulation both inter-annually and among the basin areas (Fig. 4a) make the correction relatively insignificant. We therefore report dH/dt as observed from the satellite data. From these observations, we report mass change in Table 1 and Supplement Table S2 as:

$$(dH/dt)_{\text{hyps}} \cdot (A) \cdot r \quad (2)$$

where $(dH/dt)_{\text{hyps}}$ is the elevation-band-weighted mean measured dH/dt, A is area of the glacier basin or island, and r is our assumed mean density of ice and firn lost by dynamics (900 kg m^{-3}). We eliminated the nunatak areas from each of the basins, based on the Antarctic Digital Database mapping of rock outcroppings in the region similar to previous studies (e.g., Gardner et al., 2013).

Our estimate of mass balance for the combined nAP region is -24.9 ± 7.8 Gt a^{-1}, with the great majority of the mass loss occurring at elevations below 1000 m a.s.l. (-21.9 ± 6.3 Gt a^{-1}, or 88 %; Table 1). Regionally, the eastern nAP basins dominate the mass loss at -17.7 ± 3.7 Gt a^{-1}, or 72 % of the loss, and of this, -15.0 ± 3.2 Gt a^{-1} (60 %) is from 12 glacier basins flowing into embayments formerly occupied by the Prince Gustav, Larsen Inlet, Larsen A, and Larsen B ice shelves. For the 11 western nAP glacier basins and islands, the mass loss rate at high elevation is indistinguishable from losses lower and near the coast (-2.3 ± 0.7 Gt a^{-1} > 1000 m a.s.l., and -2.2 ± 1.0 Gt a^{-1} below). Overall, the nAP region accounts for ∼29 % of Antarctica mass imbalance during the study period (Shepherd et al., 2012).

We also examined the mass balance ratio of the basins and regional areas, based on mass input, primarily snow accumulation (Lenaerts et al., 2012; Table 2, Supplement Table S3). Mass accumulation from the model (surface mass balance, or SMB) in the region has a very large gradient from west to east, with values of 1500

TCD
8, 3237–3261, 2014

to 3000 kg m^{-2} a^{-1} for the western areas and high elevations dropping to ∼500 to 1500 kg m^{-2} a^{-1} in the low elevation areas of the eastern nAP coast. A ratio of the mass balance divided by the mass accumulation input indicates the degree of imbalance in the glacier systems, and suggests the level of ice flux increase for glacier systems having recently accelerated due to ice front or ice shelf losses. We term this value the imbalance ratio. The imbalance ratio for the nAP as a whole is −0.45, implying that mass outflow is 45 % greater during the study period relative to a steady-state rate in the current climate. For the eastern nAP glaciers, the ratio is −0.3 to −3.2 (average, −0.8) with the major ISL glaciers in the Larsen A and Larsen B between −0.33 and −3.4. The upper areas of these glacier systems are essentially balanced (∼ −0.1). IFL glaciers along the western and northern coastlines have imbalance ratios similar to the ISL glaciers, ∼ −0.5 to −2.4.

Our mass balance estimate for the nAP region agrees well with recently published values, although in some cases we believe this is coincidental. Recent GRACE-based estimates that can be most easily compared with our study yield values of -27.5 ± 10 Gt a^{-1} (summing the mascons encompassing and adjacent to our study area) (Luthcke et al., 2013), and 26 ± 3 Gt a^{-1} for a larger GRACE mascon extending to 70° S (Sasgen et al., 2013). Both these GRACE-derived results inherently include portions of the Larsen C Ice Shelf and adjacent ice-covered islands we did not measure (notably, King George Island) that lost elevation and mass during the ICESat period (Gardner et al., 2013) due to the low spatial resolution of the GRACE gravimetric measurement. Similarly, the strong east-west gradient revealed in our study is not discernable by the GRACE system. Overall, however, the GRACE results provide a good summary confirmation for our study, and imply that nearly all of the mass loss for the Peninsula lies in a relatively small part of the Peninsula ice sheet (specifically, the nAP region defined here).

For earlier ICESat-only studies of the mass balance in the area (Shepherd et al., 2012), the apparent agreement is likely fortuitous. Simple extrapolation methods that do not include information about individual basin dynamics (e.g., spatial/elevation extent,

TCD
8, 3237–3261, 2014

ice shelf loss, east-west variations), lead to very different values for total mass change. We conducted two experiments using our cross-track adjusted ICESat data alone to examine the scale of possible discrepancies. With an assumption of uniform mean elevation change for each elevation band throughout the nAP the volume change from ICESat data would be $-36.6\,km^3\,a^{-1}$. This overestimate derives from ISL glaciers forming too great a part of the net elevation change measurement data, especially for their lower elevations. This is, in part, due to more ICESat data being acquired along the eastern nAP, likely a result of less cloud cover there. If one partially addresses this by separating ISL basins, the volume change is still 10 % greater than our study, $-30.6\,km^3\,a^{-1}$.

The most recent assessment of the mass balance of the Peninsula uses CryoSat-2 interferometric radar altimetry data to infer a mass balance of $-23 \pm 18\,Gt\,a^{-1}$ for a period following our evaluation, 2010–2013 (McMillan et al., 2014). The agreement is well within both studies' error bars, and suggests that mass balance for the Peninsula is not decreasing significantly at the present time.

We now examine the potential impact of further ice shelf loss in the Scar Inlet region, a remnant ice shelf section from the Larsen B Ice Shelf. Comparing high-resolution bathymetric mapping of the seabed exposed by nAP-wide ice shelf loss and glacier retreat with our data in Fig. 1 shows that it is the glaciers with deep (> 500 m) troughs and recent ice shelf loss that have the greatest elevation loss and mass imbalance (Zgur et al., 2007; Shuman et al., 2011; Rebesco et al., 2014). Recent ice-thickness maps of the tributary glaciers (Starbuck, Flask, and Leppard glaciers) of the still-intact Scar Inlet ice shelf (SIIS) indicate they have unusually deep glacier troughs just behind the grounding line, well in excess of 1000 m below sea level in the case of Flask Glacier, and −500 m a.s.l. for Starbuck glacier (Farinotti et al., 2013, 2014). From Supplement Table S5, the mean imbalance ratio of ISL glaciers with ice-front bathymetric troughs exceeding 500 m depth is −1.20, and −3.18 for regions < −1000 m a.s.l. (for comparison, it is +0.07 for trough areas > −500 m a.s.l.). If we assume that the three primary tributary glaciers of SIIS will experience the same mean imbalance ratio following a

TCD
8, 3237–3261, 2014

collapse of their frontal ice shelf in Scar Inlet, we can anticipate increased mass imbalance in those basins, from $-1.36\,\mathrm{Gt\,a^{-1}}$ during our study period to $\sim -5.5\,\mathrm{Gt\,a^{-1}}$.

5 Conclusions

Overall, our study suggests that the nAP mass imbalance pattern is a combination of several recent changes to the coastal glaciers and ice shelf systems, likely beginning several decades ago along the western coastal fjords and islands, with extensive inland propagation of mass loss to the ice divide area, and more recent ice shelf loss along the eastern flanks and islands with extensive and expanding inland propagation. Further, the large measured increase in snow accumulation over the past few decades has not created large regions of positive mass balance suggesting that negative mass balances will continue into the future.

Author Contribution

T. Scambos led the writing and compilation of graphics and final tables, and with T. Haran and J. Bohlander, conducted the ICESat-based elevation change analysis. E. Berthier conducted the differential DEM analysis and integrated the ICESat data with the dDEM data. C. Shuman and A. Cook evaluated glacier front area changes and C. Shuman produced components of Fig. 4. A. Cook provided the glacier basin outlines. S. Ligtenberg evaluated the firn compaction and accumulation variability estimates, and their impact on our results. All co-authors contributed to the writing of the paper.

The Supplement related to this article is available online at doi:10.5194/tcd-8-3237-2014-supplement.

TCD
8, 3237–3261, 2014

Acknowledgements. The ICESat data for this paper are available at the NASA Distributed Active Archive Center at NSIDC (GLA12 – GLAS/ICESat L2 Antarctic and Greenland Ice Sheet Altimetry Data). The SPOT5 HRS data were provided at no cost by CNES through the SPIRIT project. The ASTER data were provided at no cost by NASA/USGS through the Global Land Ice Measurements from Space (GLIMS) project. This work was supported by NASA grant NNX10AR76G to T. Scambos and W. Abdalati, the TOSCA and ISIS programs of the French Space Agency (CNES) to E. Berthier, NASA Cryospheric Program funds to C. Shuman, and NSF grant ANT-0732921 to T. Scambos, and the Netherlands Polar Program and European Union Seventh Framework Programme, grant 226375 to S. Ligtenberg.

References

Barrand, N. E., Vaughan, D. G., Steiner, N., Tedesco, M., Kuipers Munneke, P., van den Broeke, M. J., and Hosking, J. S.: Trends in Antarctic Peninsula surface melting conditions from observations and regional climate modeling, J. Geophys Res., 118, 315–330, doi:10.1029/2012JF002559, 2013.

Berthier, E., Scambos, T. A., and Shuman, C. A.: Mass loss of Larsen B tributary glaciers (Antarctic Peninsula) unabated since 2002, Geophys. Res. Lett., 39, L13501, doi:10.1029/2012GL051755, 2012.

Blunden, J. and Arndt, D. S.: State of the climate in 2011, B. Am. Meteorol. Soc., 93, S1–S282, doi:10.1175/2012BAMSStateoftheClimate.1, 2012.

Cook, A. J. and Vaughan, D. G.: Overview of areal changes of the ice shelves on the Antarctic Peninsula over the past 50 years, The Cryosphere, 4, 77–98, doi:10.5194/tc-4-77-2010, 2010.

Cook, A. J., Fox, A. J., Vaughan, D. G., and Ferrigno, J. G.: Retreating glacier fronts on the Antarctic Peninsula over the past half-century, Science, 308, 541–544, 2005.

Cook, A. J., Murray, T., Luckman, A., Vaughan, D. G., and Barrand, N. E.: A new 100-m Digital Elevation Model of the Antarctic Peninsula derived from ASTER Global DEM: methods and accuracy assessment, Earth Syst. Sci. Data, 4, 129–142, doi:10.5194/essd-4-129-2012, 2012.

Crist, A., Talia-Murray, M., Elking, N., Domack, E., Leventer, A., Lavoie, C., Brachfield, S., Yoo, K.-C., Gilbert, R., Jeong, S.-M., Petrushak, S., and Wellner, J.: Late Holocene glacial advance

TCD
8, 3237–3261, 2014

and ice shelf growth in Barilari 1Bay, Graham Land, west Antarctic Peninsula, Geol. Soc. Am. Bull., in press, 2014.

Dee, D. P., Uppala, S. M., Simmons, A. J., Berrisford, P., Poli, P., Kobayashi, S., Andrae, U., Balmaseda, M. A., Balsamo, G., Bauer, P., Bechtold, P., Beljaars, A. C. M., van de Berg, L., Bidlot, J., Bormann, N., Delsol, C., Dragani, R., Fuentes, M., Geer, A. J., Haimberger, L., Healy, S. B., Hersbach, H., Hólm, E. V., Isaksen, L., Kållberg, P., Köhler, M., Matricardi, M., McNally, A. P., Monge-Sanz, B. M., Morcrette, J.-J., Park, B.-K., Peubey, C., de Rosnay, P., Tavolato, C., Thépaut, J.-N. and Vitart, F.: The ERA-Interim reanalysis: configuration and performance of the data assimilation system, Q. J. Roy. Meteor. Soc., 137, 553–597, doi:10.1002/qj.828, 2011.

Farinotti, D., Corr, H., and Gudmundsson, G. H.: The ice thickness distribution of Flask Glacier, Antarctic Peninsula, determined by combining radio-echo soundings, surface velocity data and flow modelling, Ann. Glaciol., 54, 18–24, doi:10.3189/2013AoG63A603, 2013.

Farinotti, D., King, E. C., Albrecht, A., Huss, M., and Gudmundsson, G. H.: The bedrock topography of Starbuck Glacier, Antarctic Peninsula, as measured by radio-echo sounding, Ann. Glaciol., 55, 22–28, doi:10.3189/2014AoG67A025, 2014.

Favier, L., Durand, G., Cornford, S. L., Gudmundsson, G. H., Gagliardini, O., Gillet-Chaulet, F., Zwinger, T., Payne, A. J., and Le Brocq, A. M.: Retreat of Pine Island Glacier controlled by marine ice-sheet instability, Nature Climate Change, 4, 117–121, doi:10.1038/nclimate2094, 2014

Flament, T. and Rémy, F: Dynamic thinning of Antarctic glaciers from along-track repeat radar altimetry, J. Glaciol., 58, 830–840, doi:10.3189/2012JoG11J118, 2012.

Fujisada, H., Bailey, G. B., Kelly, G. G., Hara, S., and Abrams, M. J.: ASTER DEM performance, IEEE T. Geosci. Remote, 43, 2707–2714, 2005.

Gardelle, J., Berthier, E., Arnaud, Y., and Kääb, A.: Region-wide glacier mass balances over the Pamir–Karakoram–Himalaya during 1999–2011, The Cryosphere, 7, 1263–1286, doi:10.5194/tc-7-1263-2013, 2013.

Gardner, A. S., Moholdt, G., Cogley, J. G., Wouters, B., Arendt, A. A., Wahr, J., Berthier, E., Hock, R., Pfeffer, W. T., Kaser, G., Ligtenberg, S. R. M., Bolch, T., Sharp, M. J., Hagen, J. O., van den Broeke, M. R., and Paul, F.: A reconciled estimate of glacier contributions to sea level rise: 2003 to 2009, Science, 340, 852–857, doi:10.1126/science.1234532, 2013.

TCD
8, 3237–3261, 2014

Goodwin, B. P.: Recent Environmental Changes on the Antarctic Peninsula as Recorded in an ice core from the Bruce Plateau. PhD diss., The Ohio State University, Columbus, OH, 247 pp., 2013.

Haran, T., Bohlander, J., Scambos, T., and Fahnestock, M.: MODIS Mosaic of Antarctica 2004 (MOA2004) Image Map, National Snow and Ice Data Center, Boulder, Colorado USA, available at: doi:10.7265/N5ZK5DM5, 2005, updated 2014.

Howat, I. M., Joughin, I., and Scambos, T. A.: Rapid changes in ice discharge from Greenland Outlet Glaciers, Science, 315, 1559–1561, 2007.

Ivins, E. R., Watkins, M. M., Yuan, D.-N., Dietrich, R., Casassa, G., and Rülke, A.: On-land ice loss and glacial isostatic adjustment at the Drake Passage: 2003–2009, J. Geophys. Res.-Earth, 116, B02403, doi:10.1029/2010JB007607, 2011.

Joughin, I., Howat, I. M., Fahnestock, M., Smith, B., Krabill, W., Alley, R. B., Stern, H., and Truffer, M.: Continued evolution of Jakobshavn Isbrae following its rapid speedup, J. Geophys. Res.-Earth, 113, F04006, doi:10.1029/2008JF001023, 2008.

Korona, J., Berthier, E., Bernard, M., Rémy, F., and Thouvenot, E.: SPIRIT. SPOT 5 stereoscopic survey of Polar Ice: reference images and topographies during the Fourth International Polar Year (2007–2009), ISPRS J. Photogramm., 64, 204–212, doi:10.1016/j.isprsjprs.2008.10.005, 2009.

Kunz, M., King, M. A., Mills, J. P., Miller, P. E., Fox, A. J., Vaughan, D. G., and Marsh, S. H.: Multi-decadal glacier surface lowering in the Antarctic Peninsula, Geophys. Res. Lett., L19502, doi:10.1029/2012GL052823, 2012.

Lenaerts, J. T. M., van den Broeke, M. R., van de Berg, W. J., van Meijgaard, E., and Munneke, P. K.: A new, high-resolution surface mass balance map of Antarctica (1979–2010) based on regional atmospheric climate modeling, Geophys. Res. Lett., 39, L04501, 4501–4501, doi:10.1029/2011GL050713, 2012.

Ligtenberg, S. R. M., Helsen, M. M., and van den Broeke, M. R.: An improved semi-empirical model for the densification of Antarctic firn, The Cryosphere, 5, 809–819, doi:10.5194/tc-5-809-2011, 2011.

Luthcke, S. B., Sabaka, T. J., Loomis, B. D., Arendt, A. A., McCarthy, J. J., and Camp, J.: Antarctica, Greenland and Gulf of Alaska land-ice evolution from an iterated GRACE global mascon solution, J. Glaciol. 59, 613–631, doi:10.3189/2013JoG12J147, 2013.

TCD
8, 3237–3261, 2014

McMillan, M., Shepherd, A., Sundal, A., Briggs, K., Muir, A., Ridout, A., Hogg, A., and Wingham, D.: Increased ice losses from Antarctica detected by CryoSat-2, Geophys. Res. Lett. 41, 1–7, doi:10.1002/2014GL060111, 2014.
Mulvaney, R., Abram, N. J., Hindmarsh, R. C., Arrowsmith, C., Fleet, L., Triest, J., and Foord, S.: Recent Antarctic Peninsula warming relative to Holocene climate and ice-shelf history, Nature, 489, 7414, 141–144, doi:10.1038/nature11391, 2012.
Nick, F. M., Vieli, A., Howat, I. M., and Joughin, I.: Large-scale changes in Greenland outlet glacier dynamics triggered at the terminus, Nat. Geosci., 2, 110–114, 2009.
Pfeffer, W. T.: A simple mechanism for irreversible tidewater glacier retreat, J. Geophys. Res.-Earth, 112, F03S25, doi:10.1029/2006JF000590, 2007.
Potocki, M., Mayewski, P. A., Kurbatov, A., Handley, M., Simoes, J. C., and Jaña, R.: Detailed glaciochemical records from a northern Antarctic Peninsula site-Detroit Plateau. In AGU Fall Meeting Abstracts, 1, p. 1822, 2011, San Francisco, 5–9 December, 2011.
Pritchard, H. D. and Vaughan, D. G.: Widespread acceleration of tidewater glaciers on the Antarctic Peninsula, J. Geophys. Res.-Earth, 112, F03S29, doi:10.1029/2006JF000597, 2007.
Pritchard, H. D., Arthern, R. J., Vaughan, D. G., and Edwards, L. A.: Extensive dynamic thinning on the margins of the Greenland and Antarctic ice sheets, Nature, 461, 971–975, 2009.
Pritchard, H. D., Ligtenberg, S. R. M., Fricker, H. A., Vaughan, D. G., van den Broeke, M. R., and Padman, L.: Antarctic ice-sheet loss driven by basal melting of ice shelves, Nature, 484, 7395, 502–505, doi:10.1038/nature10968, 2012.
Rebesco, M., Domack, E., Zgur, F., Leventer, A., Lavoie, C., Brachfeld, S., Willmott, V., Halverson, G., Truffer, M., Scambos, T., and Smith, J.: Boundary condition of grounding lines prior to collapse, Larsen-B Ice Shelf, Antarctica. Science, in review, 2014.
Rignot, E., Casassa, G., Gogineni, P., Krabill, W., Rivera, A., and Thomas, R.: Accelerated ice discharge from the Antarctic Peninsula following the collapse of Larsen B ice shelf, Geophys. Res. Lett., 31, L18401, doi:10.1029/2004GL020697, 2004.
Rignot, E., Bamber, J. L., van den Broeke, M. R., Davis, C., Li, Y. H., van de Berg, J., and van Meijgaard, E.: Recent Antarctic ice mass loss from radar interferometry and regional climate modelling, Nat. Geosci., 1, 106–110, doi:10.1038/ngeo102, 2008.
Rott, H., Müller, F., Nagler, T., and Floricioiu, D.: The imbalance of glaciers after disintegration of Larsen-B ice shelf, Antarctic Peninsula, The Cryosphere, 5, 125–134, doi:10.5194/tc-5-125-2011, 2011.

TCD
8, 3237–3261, 2014

Saha, S., Moorthi, S., Wu, X., Wang, J., Nadiga, S., Tripp, P., Behringer, D., Hou, Y.-T., Chuang, H.-Y., Iredell, M., Ek, M., Meng, J., Yang„ R., Mendez, M. P., van den Dool, H., Zhang, Q., Wang, W., Chen, M., and Becker, E.: The NCEP climate forecast system version 2, J. Climate, 27, doi:10.1175/JCLI-D-12-00823.1, 2013.

Sasgen, I., Konrad, H., Ivins, E. R., Van den Broeke, M. R., Bamber, J. L., Martinec, Z., and Klemann, V.: Antarctic ice-mass balance 2003 to 2012: regional reanalysis of GRACE satellite gravimetry measurements with improved estimate of glacial-isostatic adjustment based on GPS uplift rates, The Cryosphere, 7, 1499–1512, doi:10.5194/tc-7-1499-2013, 2013.

Scambos, T. A., Haran, T. M., Fahnestock, M. A., Painter, T. H., and Bohlander, J.: MODIS-based Mosaic of Antarctica (MOA) data sets: continent-wide surface morphology and snow grain size, Remote Sens. Environ., 111, 242–257, 2007.

Schutz, B. E., Zwally, H. J., Shuman, C. A., Hancock, D., and DiMarzio, J. P.: Overview of the ICESat mission, Geophys. Res. Lett., 32, L21S01, doi:10.1029/2005GL024009, 2005.

Shepherd, A., Ivins, E. R., A, G., V. R., Bentley, M. J., Bettadpur, S., Briggs, K., Bromwich, D. H., Forsberg, R., Galin, N., Horwath, M., Jacobs, S., Joughin, I., King, M. A., Lenaerts, J. T. M., Li, J., Ligtenberg, S. R. M., Luckman, A., Luthcke, S. B., McMillan, M., Meister, R., Milne, G., Mouginot, J., Muir, A., Nicolas, J. P., Paden, J., Payne, A. J., Pritchard, H., Rignot, E., Rott, H., Sørensen, L. S., Scambos, T. A., Scheuchl, B., Schrama, E. J. O., Smith, B., Sundal, A. V., J. H., van de Berg, W. J., van den Broeke, M. R., Vaughan, D. G., Velicogna, I., Wahr, J., Whitehouse P. L., Wingham, D. J., Yi, D., Young, D., and Zwally, H. J.: A Reconciled Estimate of Ice-Sheet Mass Balance, Science, 338, 1183–1189, doi:10.1126/science.1228102, 2012.

Shuman, C. A., Zwally, H. J., Schutz, B. E., Brenner, A. C., DiMarzio, J. P., Suchdeo, V. P., and Fricker, H. A.: ICESat Antarctic elevation data: preliminary precision and accuracy assessment, Geophys. Res. Lett., 33, L07501, doi:10.1029/2005GL025227, 2007.

Shuman, C. A., Berthier, E., and Scambos, T. A.: 2001–2009 elevation and mass losses in the Larsen A and B embayments, Antarctic Peninsula, J. Glaciol., 57, 737–754, doi:10.3189/002214311797409811, 2011.

Stammerjohn, S. E., Martinson, D. G., Smith, R. C., Yuan, X., and Rind, D.: Trends in Antarctic annual sea ice retreat and advance and their relation to El Niño-Southern Oscillation and Southern Annular Mode variability, J. Geophys. Res.-Oceans (1978–2012), 113, C03S90, doi:10.1029/2007JC004269, 2008.

van den Broeke, M.: Strong surface melting preceded collapse of Antarctic Peninsula ice shelf, Geophys. Res. Lett., 32, L12815, doi:10.1029/2005GL023247, 2005.

TCD
8, 3237–3261, 2014

Zagorodnov, V., Nagornov, O., Scambos, T. A., Muto, A., Mosley-Thompson, E., Pettit, E. C., and Tyuflin, S.: Borehole temperatures reveal details of 20th century warming at Bruce Plateau, Antarctic Peninsula, The Cryosphere, 6, 675–686, doi:10.5194/tc-6-675-2012, 2012.

Zgur, F., Rebesco, M., Domack, E. W., Leventer, A., Brachfeld, S., and Willmott, V.: Geophysical survey of the thick, expanded sedimentary fill of the new-born Crane fjord (former Larsen B Ice Shelf, Antarctica), US Geol. Surv. Open File Rep. 1047, 2007.

TCD
8, 3237–3261, 2014

Table 1. Summary of Mass Balance for the northern Antarctic Peninsula, 2001–2010. Units: Area (km^2), Mean dM/dt ($Gt\,a^{-1}$), Number of Measurements, Mean dh/dt ($m\,a^{-1}$), Mean dV/dt ($km^3\,a^{-1}$).

Region	Ice-Covered Area	Total dM/dt[a]	Ice Front Retreat Area[b]	dh/dt[c]	dV/dt[d,h]	Below 1000 m a.s.l. Area	dDEM[e]	ICESat[f]	dh/dt[g]	dV/dt[h]	Above 1000 m a.s.l. Area	ICESat[f]	dh/dt[g]	dV/dt[h]
nAP < 66° S, 1–33	**34 232.8**	**−24.9**	**325.6**	**−3.5**	**−1.2**	**23 582.6**	**44.8**	**12 476**	**−1.00**	**−23.1**	**10 651.7**	**2668**	**−0.31**	**−3.4**
nAP West, 1–11	**14 338.2**	**−4.8**	**7.8**	**−5.3**	**−0.2**	**9014.3**	**38.6**	**2999**	**−0.27**	**−2.4**	**5323.7**	**893**	**−0.59**	**−2.8**
nAP North, 12–14	**3688.0**	**−2.4**	**4.0**	**−3.3**	**−0.1**	**3684.3**	**8.2**	**2204**	**−0.69**	**−2.5**	**3.7**	**(0)**	**(−0.31)**	**0.0**
nAP East, 15–33	**16 207.5**	**−17.7**	**313.8**	**−5.7**	**−0.9**	**10 884.0**	**62.4**	**7279**	**−1.67**	**−18.2**	**5323.5**	**1775**	**−0.10**	**−0.6**
Northwest AP Coast[i]	5255.1	−1.7	–	–	–	3417.9	35.1	1270	−0.27	0.9	1837.0	575	−0.50	−0.9
Western IFL Glaciers[j]	**679.4**	**−1.1**	**11.8**	**−4.6**	**−0.03**	**452.1**	**35.6**	**450**	**−2.24**	**−1.0**	**226.5**	**(0)**	**(−0.84)**	**−0.2**
Eastern ISL Glaciers[k]	**9262.3**	**−15.0**	**305.7**	**−5.9**	**−0.90**	**6030.9**	**70.9**	**3903**	**−2.60**	**−15.7**	**3232.6**	**941**	**−0.01**	**−0.2**
James Ross Island[l]	1800.8	−2.4	47.1	−3.3	−0.08	1380.0	58.0	417	−1.93	−2.7	420.7	215	0.02	0.0
Prince Gustav tributaries[m]	1885.0	−2.7	58.2	−3.6	−0.10	1478.4	76.6	475	−2.03	−3.0	406.7	123	0.23	0.1
Larsen A tributaries[n]	3184.4	−4.9	29.3	−2.7	−0.04	2094.8	85.5	1594	−2.32	−4.9	1089.7	329	−0.08	−0.1
Larsen B ISL tributaries[o]	4192.9	−7.9	218.2	−3.9	−0.82	2457.7	55.2	1834	−3.18	−7.8	1736.2	489	−0.13	−0.2
Scar Inlet Ice Shelf trib.[p]	3524.5	−1.4	–	–	–	2089.8	46.4	1965	−0.47	−0.7	1434.7	715	−0.37	−0.5

Abbreviations for place names: nAP, northern Antarctic Peninsula; ISL, ice shelf loss; IFL, ice front loss.

[a] Assuming mean density of 900 $kg\,m^{-3}$ for all dV/dt measurements. Errors for these values are 0.9 times the sum of errors for dV/dt for each row.

[b] Area determined from additional ASTER, SPOT, and Landsat images, spanning 2000–2002 to 2009–2010.

[c] Rate of elevation loss measured just above area of grounded ice retreat.

[d] Volume loss assumes flotation was reached midway between 2001–2010 (period of observations).

[e] Percent area covered by differential DEM satellite stereo-image data.

[f] Number of repeat-track point measurements used. If < 10 ICESat dH/dt measurements are available, the regional mean ICESat dH/dt for areas > 1000 m ($-0.31\,m\,a^{-1}$) or, for sub-basins, the main basin mean, is used.

[g] Hypsometric weighting for areas below 1000 m elevation; weighted by number of ICESat measurements for areas above 1000 m elevation.

[h] Errors on dV/dt can be determined by: $\pm 0.3\,m\,a^{-1}$ · area for regions ≤ 1000 m a.s.l. (dDEM and ICESat data) and $\pm 0.15\,m\,a^{-1}$ · area for regions > 1000 m a.s.l. (ICESat data).

[i] Glacier basins 8–11.

[j] Glacier basins 1a, 4a, 6a, and 12a.

[k] Glacier basins 19, 21–25, 26b, 27–30, and 31a.

[l] Glacier basins 17, 18, and 19.

[m] Glacier basins 19 and 21.

[n] Glacier basins 22–25.

[o] Glacier basins 26b, 27–30, and 31a.

[p] Glacier basins 31b, 32, and 33.

TCD
8, 3237–3261, 2014

Table 2. Comparison of total mass balance (dM/dt), input surface mass (dM_i/dt), and resulting imbalance ratio. Units: Area (km^2); dM/dt, $Gt\,a^{-1}$; Mean dh/dt, $m\,a^{-1}$; SMB, $kg\,m^{-2}\,a^{-1}$; dM_i/dt, $Gt\,a^{-1}$.

Region	Ice-Covered Area	Total dM/dt	Mean dh/dt	Mean SMB	Total dM_i/dt	**Imbal. ratio**	< 1000 dh/dt	< 1000 SMB	< 1000 dM_i/dt	**< 1000 ratio**	> 1000 dh/dt	> 1000 SMB	> 1000 dM_i/dt	**> 1000 ratio**
nAP < 66° S, 1–33	34 232.8	−24.8	−0.77	1543	54.2	**−0.45**	−1.00	1295	29.9	**−0.70**	−0.31	2104	23.1	**−0.18**
nAP West, 1–11	14 337.3	−4.6	−0.33	2112	30.4	**−0.14**	−0.27	1964	17.7	**−0.12**	−0.59	2361	12.6	**−0.17**
nAP North, 12–14	3688.0	−2.4	−0.69	537	2.0	**−1.15**	−0.69	537	2.0	**−1.15**	(−0.31)	920	0.0	**–**
nAP East, 15–33	16 207.6	−17.8	−1.20	1268	21.8	**−0.81**	−1.75	1007	10.5	**−1.56**	−0.10	1844	9.8	**−0.06**
Northwest AP Coast[a]	5255.1	−1.7	−0.35	2012	10.6	**−0.16**	−0.27	1770	6.0	**0.13**	−0.51	2458	4.5	**−0.18**
Western IFL Glaciers[b]	**679.4**	**−1.1**	**−1.77**	**1839**	**1.2**	**−1.26**	**−2.24**	**1484**	**0.7**	**−1.29**	**−0.83**	**2546**	**0.6**	**−0.28**
Eastern ISL Glaciers[c]	**9262.3**	**−15.0**	**−1.66**	**1399**	**13.0**	**−1.15**	**−2.60**	**1143**	**6.9**	**−2.05**	**−0.07**	**1898**	**6.1**	**−0.04**
James Ross Island[d]	1800.8	−2.4	−1.44	689	1.2	**−2.09**	−1.93	653	0.9	**−2.70**	0.02	834	0.4	**0.00**
Prince Gustav tributaries[e]	1885.0	−2.7	−1.54	1173	2.2	**−1.23**	−2.03	968	1.4	**−1.93**	0.21	2003	0.8	**0.10**
Larsen A tributaries[f]	3184.4	−4.9	−1.55	1624	5.2	**−0.94**	−2.32	1358	2.8	**−1.58**	−0.08	2154	2.3	**−0.03**
Larsen B ISL tributaries[g]	4192.9	−7.9	−1.80	1329	5.6	**−1.42**	−3.18	1064	2.6	**−2.68**	−0.13	1713	3.0	**−0.07**
Scar Inlet Ice Shelf trib.[h]	3524.5	−1.4	−0.42	1296	4.6	**−0.30**	−0.47	787	1.6	**−0.38**	−0.37	2049	2.9	**−0.16**

[a] Glacier basins 8–11.
[b] Glacier basins 1a, 4a, 6a, and 12a.
[c] Glacier basins 19, 21–25, 26b, 27–30, and 31a.
[d] Glacier basins 17, 18, and 19.
[e] Glacier basins 19 and 21.
[f] Glacier basins 22–25.
[g] Glacier basins 26b, 27–30, and 31a.
[h] Glacier basins 31b, 32, and 33.

TCD
8, 3237–3261, 2014

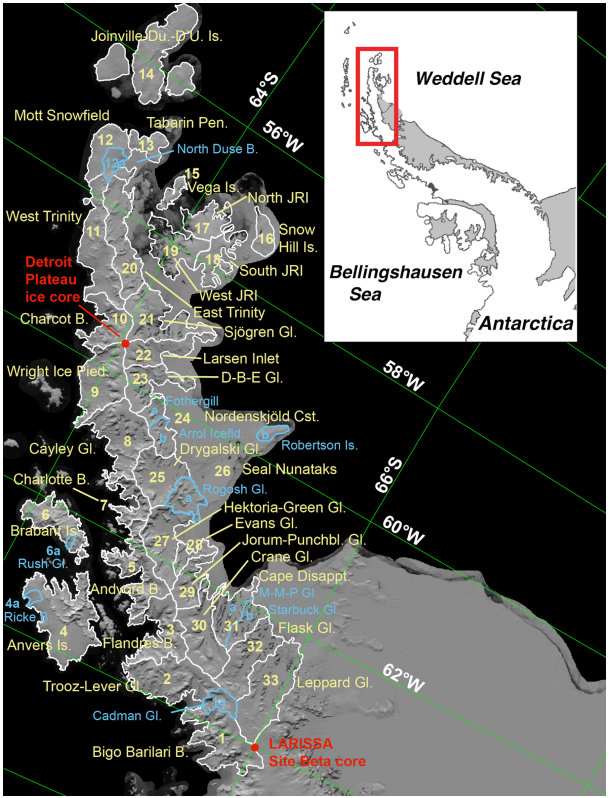

Figure 1. Location and outline of basins and sub-basins in the study area, and sites of two climate ice cores discussed in the text. Region names, basin numbers, and abbreviations are the same as in Supplement Tables S2 and S3. Major drainage basins are outlined in white, sub-basins are indicated in blue. Base image is the MODIS Mosaic of Antarctica (Scambos et al., 2007). Inset, location of the study area shown in Fig. 2.

TCD
8, 3237–3261, 2014

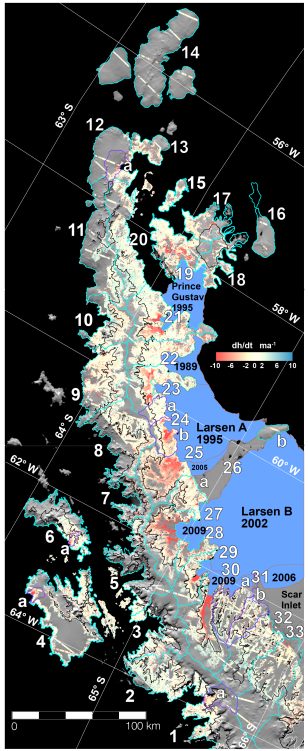

Figure 2. Elevation change rates (dH/dt) and major and minor glacier basin or islands for the northern Antarctic Peninsula study area. Cyan outlines indicate the measured study basins and islands; surrounding numbers and letters refer to Supplement Tables S2 and S3 entries. Magenta outlines with lower-case labels identify sub-basins within a major basin where a separate hypsometric interpolation is used. Black contour line indicates 1000 m a.s.l. elevation. Major ice shelf retreat areas since 1980 (Cook and Vaughan, 2010) are indicated in blue, with years of major collapse events and the limit of extensive grounded ice loss shown. Ice edge is from a 2009 MODIS mosaic (Haran et al., 2014).

TCD
8, 3237–3261, 2014

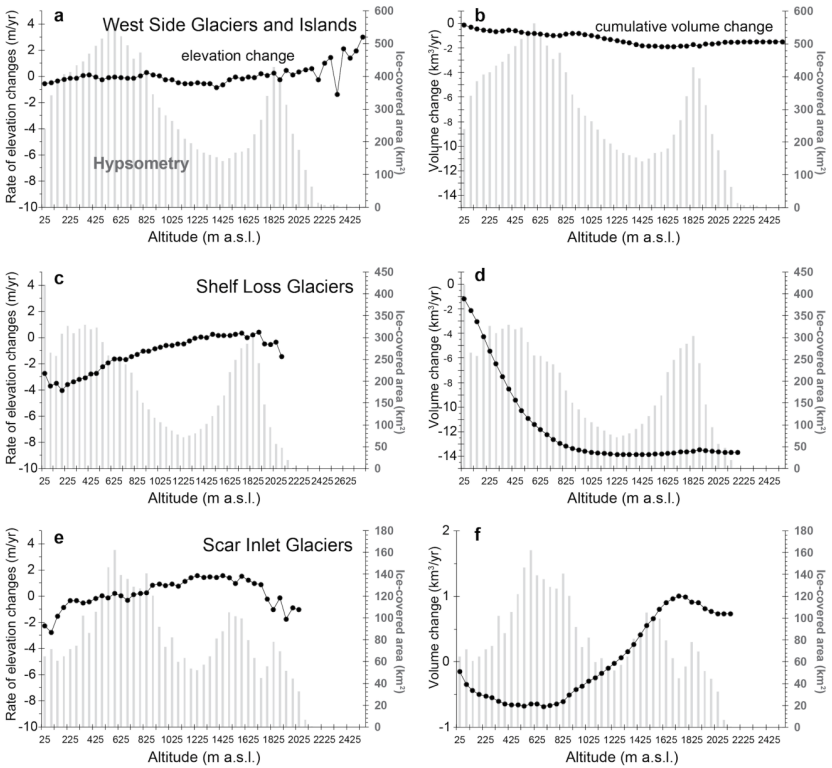

Figure 3. Hypsometry of elevation and volume changes of western basins (**a** and **b**; basins 1–11 in Table 1), eastern basins with major ice shelf loss in the period 1986–2009 (**c** and **d**; basins 19, 21–25, and 27–30 in Table 1), and basins draining to the Scar Inlet ice shelf area (**e** and **f**; basins 31b, 32, and 33 in Table 1). Height is binned in 50 m intervals. Note that rates of elevation change trends at the highest elevations (> 2000 m a.s.l., right side of left column of panels) are based on few data and are not reliable.

TCD
8, 3237–3261, 2014

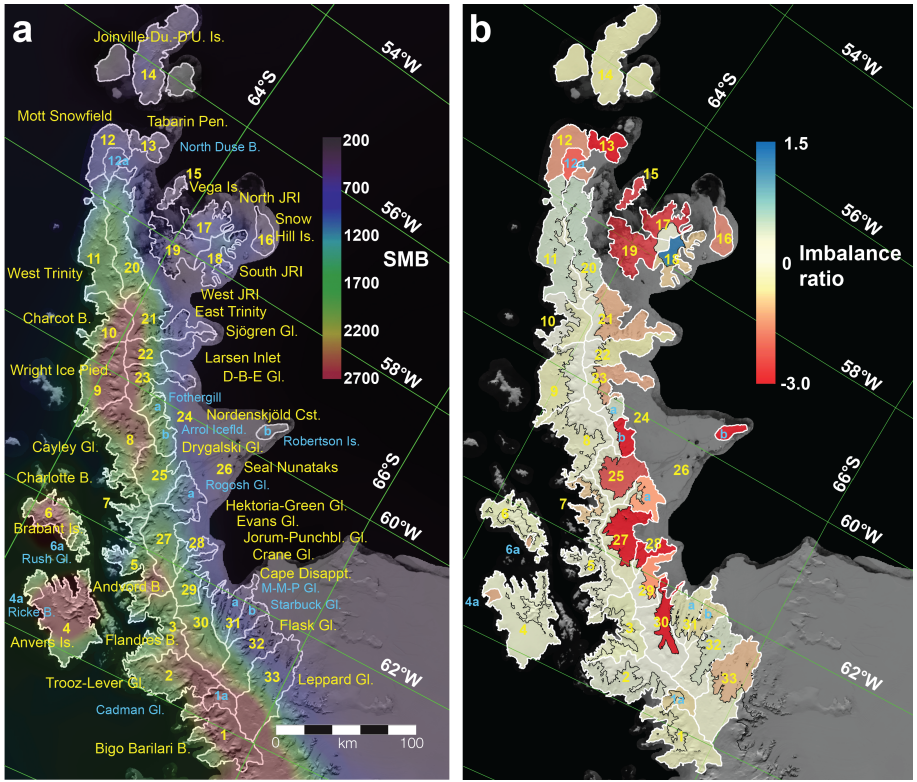

Figure 4. Comparison of the study area basin extents with RACMO-2 estimated SMB in $kg\,m^{-2}\,a^{-1}$ **(a)** and mass imbalance ratio for the basin areas separated by high and low elevation areas (above and below 1000 m; **b**).

TCD
8, 3237–3261, 2014